

This document was prepared in conjunction with work accomplished under Contract No. DE-AC09-76SR00001 with the U.S. Department of Energy.

DISCLAIMER

This report was prepared as an account of work sponsored by an agency of the United States Government. Neither the United States Government nor any agency thereof, nor any of their employees, makes any warranty, express or implied, or assumes any legal liability or responsibility for the accuracy, completeness, or usefulness of any information, apparatus, product or process disclosed, or represents that its use would not infringe privately owned rights. Reference herein to any specific commercial product, process or service by trade name, trademark, manufacturer, or otherwise does not necessarily constitute or imply its endorsement, recommendation, or favoring by the United States Government or any agency thereof. The views and opinions of authors expressed herein do not necessarily state or reflect those of the United States Government or any agency thereof.

This report has been reproduced directly from the best available copy.

Available for sale to the public, in paper, from: U.S. Department of Commerce, National Technical Information Service, 5285 Port Royal Road, Springfield, VA 22161, phone: (800) 553-6847, fax: (703) 605-6900, email: orders@ntis.fedworld.gov online ordering: <http://www.ntis.gov/ordering.htm>

Available electronically at <http://www.doe.gov/bridge>

Available for a processing fee to U.S. Department of Energy and its contractors, in paper, from: U.S. Department of Energy, Office of Scientific and Technical Information, P.O. Box 62, Oak Ridge, TN 37831-0062, phone: (865) 576-8401, fax: (865) 576-5728, email: reports@adonis.osti.gov

TECHNICAL DIVISION
SAVANNAH RIVER LABORATORY

DPST-83-553

ACC. NO. 103603

DISTRIBUTION

J. L. WOMACK, 703-A, SRP
G. F. MERZ, 703-A,
L. HIBBARD, 703-A
C. P. ROSS, 703-A
W. B. DASPIT, 706-C
M. M. ANDERSON, 703-A
F. D. BENTON, 706-C
F. BERANEK, 706-C
C. E. AHLFELD, 706-C
S. P. RIDEOUT, 704-M
N. H. KUEHN, 706-C
R. L. FRONTROTH, 777-10A

S. E. ALEMAN, 706-C
W. M. MASSEY, 706-C
S. MIRSHAK, 773-A
J. W. STEWART, 773-A, SRL
D. A. WARD, 773-A
M. R. BUCKNER, 773-A
D. W. PEPPER, 786-1A
C. B. JONES, 773-A
D. A. SHARP, 773-24A
H. B. PEACOCK, 773-A
L. L. HAMM, 786-1A
SRL RECORDS (4)

May 27, 1983

TO: M. R. BUCKNER

FROM: J. E. MCALLISTER, JR. ^{g.e.m.}

TIS FILE
RECORD COPY

HEAT TRANSFER CHARACTERISTICS OF MARK 15 SLUGS FOR DIFFERENT
BONDING CONDITIONS

INTRODUCTION

The limits parameters for Mark 15 operation¹ assume that the core and cladding are adequately bonded. No allowance is made for a nonbond in calculating the burnout risk² (BOR), which is consistent with other slug type assemblies at SRP. Poor bonds cause peaks in the heat flux from slugs which adversely affect BOR. A new test for bond quality in the 300 area, however, indicates that the initial run of Mark 15 outer slugs did have a poor bond around the endcap region. A model was developed to determine the changes in the heat transfer characteristics of the Mark 15 outer slug for the poor bonds seen in the 300 area tests.

SUMMARY

A numerical heat transfer model based on the HEATING5³

conduction code was developed to analyze poor bonding around the endcap of the outer Mark 15 slug. An analytical model could not be developed because of non-uniform heat generation in the core and the arrangement of the various materials in the cylindrical geometry. For the conservative case where the poor bond region extends 1.5 in. from the endcap, is 0.5 mils thick, and is modeled as aluminum oxide, the heat flux peak is 2.6%. The increase in BOR for this case is negligible and will not reduce reactor power during the July, 1983 irradiation. Results for air gaps are also included; however, they are not considered reasonable poor bond cases because the 300 area inspection tests can detect slugs with air gaps.

DISCUSSION

Background

Tests in the 300 area indicate that the bond at the nickel-aluminum interface on the outer Mark 15 slugs has a low tensile strength. This poor bond region occurs around the endcap region and is attributed to poor diffusion between the aluminum can and nickel plate during the hot die sizing process.

Figure 1 shows the region characterized by a poor bond. Analysis by a microprobe, electron microscope, and stud pull tests indicate that the oxide layer thickness is negligible (less than 0.01 mil in the poor bond region).

An oxide layer thickness of up to 0.5 mil has been found in some slugs, but these slugs had been rejected during the normal inspection process conducted in the 300 area. The problem is how to model the poor bond region where the thermal conductivity values are expected to be less than the values for a pure metal-to-metal contact. Since the maximum poor bond width on rejected slugs was on the order of 0.5 mils, the maximum value for a poor bond width in the model was assumed to be 0.5 mil. More typical width values in Figure 1 would be less than 0.5 mils. The material in the poor bond region was assumed to be either aluminum or uranium oxide.

In the results section, poor bond widths were assumed to be either 0.5 mils or 0.25 mils for different Z values and oxide types with different poor bond scenarios. The poor bond region in Figure 1 is composed of three separate areas. The different poor bond scenarios assumed

- o All three poor bond regions present.
- o The poor bond region on only the outer core circumference or on only the top of the core.

- o Poor bond regions on both the inner and outer circumferences.

Additional results are also presented where the poor bond region is actually an air gap for a variety of gap thicknesses, Z values, and region combinations. The air gap cases are unrealistic since the normal inspection process would eliminate these slugs before they were put into the reactor.

The numerical model will predict conservative, i.e., higher than expected, hot spots because

- o The poor bond regions extend around the entire core circumference. Destructive tests on the Mark 15 outer slugs indicate that this situation rarely happens.
- o Poor bond widths are assumed to be either 0.25 mils or 0.5 mils. Widths of this magnitude would not pass the quality control tests in the 300 area. More realistic widths are less than 0.1 mils.

Figure 2 shows the expected heat flow path out of an outer slug for a good and poor bond. In this figure, the magnitude of the heat flow is represented by the boldness of the arrows. The good bond case shows larger heat flow paths towards the top of the core, which is expected because of the increased heat generation in this region. For the poor bond case, the poor bond region inhibits heat flow. As a result, the heat flow through the poor bond area is small. As shown in Figure 2, the heat flow from the upper core region moves down the core and around the lower end of the poor bond region. The peak heat flux will generally occur on the clad surface at the lower end of the poor bond region. The peak in heat flux moves above the lower poor bond boundary when the poor bond width is small enough that the resistance to heat flow becomes negligible.

Numerical Model

The outer Mark 15 slug is a simple cylinder with an aluminum clad surrounding a uranium core. Due to symmetry, only half of the cylinder needs to be modeled. The computer model was developed for the HEATING5³ computer code. HEATING5 is a general purpose heat conduction code capable of handling a variety of standard geometries. Figure 1 shows the upper half of a standard Mark 15 outer slug. This slug was initially modeled² without the poor bond regions to determine the heat flux peak due to the Wilkins effect.

The heat generation in the slug varies⁴ radially and axially. As seen in Figure 1, the core was divided into five

regions which are numbered. Table 1 lists the variation in heat generation for these five regions normalized with respect to the axial midplane of the slug. Table 2 lists the relative power of each region.

Table 3 lists the thermal conductivities that were used. Since the value for aluminum oxide was reported as 1.3 ± 0.2 , the lowest (conservative) value of 1.1 was used. The thermal conductivity for uranium oxide, UO_2 , is temperature dependent and decreases with increasing temperature. Results indicate UO_2 is less than $200^\circ C$; the UO_2 thermal conductivity value in Table 3 is conservative.

Two checks on the validity of the numerical results are

- o Increase the number of nodes
- o A more stringent error criteria

The numerical results for the Figure 1 geometry were obtained for 1053, 1092, 1242, and 2652 nodes. Negligible differences in the maximum core and clad surface temperatures were obtained for the different meshes. The error criteria is

$$\text{error} = \frac{T_i - T_{i-1}}{T_{i-1}}$$

where

T = temperature at i^{th} iteration

The error criteria is calculated for each node. For a given error criteria, the HEATING5 code iterates until the maximum error criteria for all the nodes is less than the specified error criteria value in the input data. The error criteria in this study was varied from 10^{-7} to 10^{-9} with no changes in the predicted temperatures.

Due to symmetry, the heat transfer from the midplane in Figure 1 is zero. Since slugs are placed on top one another in the reactor, no heat transfer occurs off the endcap. As a result, the only heat transfer from the slug in Figure 1 is off the inner and outer slug surfaces. The boundary conditions on the inner and outer slug surface were determined from the CREDIT' code by assuming a nominal assembly power.

Table 4 lists the channel coolant temperatures and convection heat transfer coefficients for the two assembly powers considered in this study. Initially, the 6.12 MW power was chosen because it is a representative Mark 15 assembly power. The 7.82 MW power

represents an assembly comprised of 18 slugs, each running at the power of the hottest slug in the reactor.

The numerical model considers heat generation as varying both radially and axially. Because of this treatment, the hot spot factors in this document can be thought of as increases in the Wilkins effect. When calculating the new BOR curves, the only change in the input data is to increase the uncertainty due to the Wilkins effect.

Results

For the good bond case, Figure 3 shows temperatures at various points in the r-z plane. The maximum core temperature is 236°, which occurs in the upper region of the core. The location in all the figures of the maximum core temperature is only an approximation as this temperature does not always occur in the same location. The maximum inner and outer slug surface temperatures, 135°C and 136°C, are shown because the increase in the hot spot is related to these temperature values by

$$\text{Hot Spot} = \frac{(T_s - T_c)h}{(T_{sw} - T_c)h}$$

where

T_s = Maximum surface temperature for the poor bond scenario

T_c = Coolant channel temperature

T_{sw} = Maximum surface temperature for the standard case, which considers the Wilkins effect

h = Convection coefficient

The convection coefficient is a function of the coolant and metal surface temperatures. The two h values in the previous equation were assumed to be equal because of the small differences in the surface temperatures for the realistic poor bond scenarios. The 160°C and 161°C temperatures in Figure 3 represent the core temperature at the closest node to the maximum slug surface temperatures. When comparing the numbers for this node for the various cases, true comparisons should only be based on runs with the same number of nodes. For cases with more nodes, the core node represented by 155°C in Figure 6 is closer to the aluminum clad than the 160°C node in Figure 3, which is for a 1092 node case. The inner and outer slug surface temperatures in Figure 3 are not expected to be equal because

- o The channel coolant temperature and convection heat transfer coefficient on the inner and outer surfaces are not equal.
- o The heat generation is non-uniform in both the axial and radial directions.

The upper half of the slug in Figure 1 is 4.36 in. long. In the various poor bond cases considered, only the upper portion (maximum Z is 1.5 in.) of the slug is altered. Because of the high convection heat transfer rates, perturbations to the heat transfer characteristics of the upper region of the core are smoothed out in relatively short distances from the poor bond regions. All the cases which were considered verified this reasoning. The midplane temperatures - 134°C, 231°C, and 135°C in Figure 3 - were unchanged for all the cases. Figures 4 and 5 show the variation in inner slug surface temperature for four different poor bond scenarios.

Figures 6 and 7 show the temperature differences for the 6.12 MW and 7.82 MW slug powers. Using the poor bond region in these two figures is the most restrictive of the region combinations considered because this case produces the worst (highest) hot spot factors. The poor bond parameters in both figures are identical and in the same column to enable quick comparisons between the two figures. The cases for air as the gap material are intended to show the dramatic increase in hot spot factor when air is present. Assuming aluminum oxide as the gap material is also conservative since all the tests on Mark 15 outer slugs indicate that if any oxide is present for these gap widths, it is uranium oxide with a thermal conductivity of 3.15 pcu/hr-ft-°C. Higher conductivity values in the poor bond region permit more heat flow off the outer slug surface, which lowers the hot spot factor on the inner surface. The temperature distributions in Figure 5 are for the 0.5 mil cases of Figure 6.

The small differences in the hot spot factors for Figures 6 and 7 show that the variation in slug power has little effect on hot spot value. The hot spot values are based on the maximum surface temperatures which are shown in Figures 6 and 7. For example, the maximum surface temperature for the 0.5 mil aluminum oxide case in Figure 6 is 137°C. The relative ranking of the hot spot factors in Figure 6 and 7 are physically realistic since

- o Larger gaps result in larger hot spot values.
- o A lower thermal conductivity material (larger resistance to heat flow) results in larger hot spot values.

Figures 8 and 9 are for two additional poor bond combinations. The hot spot values in these cases are lower than the values in Figure 6, which is at the same 6.12 MW power, for similar poor bond parameters.

Figures 10 and 11 show hot spot factors for a variety of poor bond scenarios. The only realistic case in these figures is the 0.5 mil nickel oxide case of Figure 11. Since the thermal conductivity of nickel oxide could not be found, its value was conservatively estimated to be 0.3 pcu/hr-ft-°C. This value is well below the conductivity values for uranium oxide and aluminum oxide. As a result, if nickel oxide was actually present the temperatures in Figure 11 for this case would be higher than what would actually occur.

In Figures 10 and 11, radiative heat transfer across the air gap was permitted except where noted. The radiative heat transfer was modeled by

$$\begin{aligned} Q_R &= F_{12} \epsilon_1 \epsilon_2 \sigma (T_1^4 - T_2^4) \\ &= h_r (T_1^4 - T_2^4) \end{aligned}$$

where

- Q_R = radiative heat transfer
- F_{12} = shape factor = 1
- ϵ_1 = emissivity of oxidized uranium, equal 0.5
- ϵ_2 = emissivity of oxidized aluminum, equal 0.2
- σ = Stefan-Boltzman constant, 0.1714 Btu/hr-°R⁴-ft²
- h_r = radiative heat transfer coefficient input into HEATING5
- T_1 = core temperature
- T_2 = aluminum clad temperature

No radiative heat transfer was permitted across the air gaps in Figures 6 and 7.

Figure 13 shows the effect of permitting an air gap across the top of the core around the entire slug circumference. The effect is negligible which is not unexpected since no heat transfer is permitted off the slug endcap. The air gap in Figure 13 is insulating a portion of the slug which does not have much heat flow.

In comparing the maximum core temperatures in Figures 6-11, no unusual (unrealistic) temperatures were calculated by the model. The following generalizations are helpful in these comparisons:

- o Lower Z values cause lower core temperatures.
- o Larger gap widths cause higher core temperatures.
- o Lower thermal conductivities cause higher core temperatures.
- o More poor bond regions cause higher core temperatures. For example, Figure 6 has one poor bond region while Figure 10 has two regions.

In summary, the maximum hot spot factor for a realistic poor bond scenario (no air) is 1.026 from Figure 7. Allowing for some uncertainty in this value, the Wilkins effect uncertainty values were increased by 3% (hot spot of 1.03) and a new burnout risk curve was calculated. Figure 12 shows the Mark 15 BOR curves from Reference 7 and the new BOR curve for the outer surface of the inner slug. The increase in burnout risk is very small and will not reduce reactor power for the July, 1983 irradiation if it is necessary to use MK-15 slugs with poor bonds of the type analyzed.

REFERENCES

1. McAllister, J. E., "BOR, HCF, T_{mnf} , and General Heat Transfer Characteristics of the Mark 15 Assembly," DPST-83-446, April 14, 1983.
2. Hamm, L. L. and J. E. McAllister, Jr., "Uncertainties Affecting $BOSF_N$ for the Mark 15 Assembly," DPST-83-xxx to be issued.
3. Turner, W. D., Elrod, D. C. and I. I. Siman-Twoo, HEATING5 - An IBM 360 Heat Conduction Program, ORNL/CSD/TM-15, Union Carbide Corp., Oak Ridge, Tenn.
4. O'Kula, K. R., "Flux Peaking Calculations for Mark 15 Assemblies," DPST-83-411, to be issued.
5. Ondrejcin, R. S., "Evaluation of Mark 22 Cladding," DPST-83-324, March 23, 1983.
6. Foster, A. R. and R. L. Wright, Jr., Basic Nuclear Engineering, Allyn and Bacon, Inc., Boston, Mass., 1977, p. 365.
7. McAllister, J. E., Knight, J. F. and L. L. Hamm, "CREDIT Documentation and the Mark 15 Subroutine," DPST-83-402, March 31, 1983.

TABLE 1

AXIAL HEAT GENERATION IN THE OUTER MARK 15 SLUG

<u>Distance From Midplane, in.</u>	Normalized Heat Generation Region				
	<u>1</u>	<u>2</u>	<u>3</u>	<u>4</u>	<u>5</u>
0.0	1.0000	1.0000	1.0000	1.0000	1.0000
0.54	1.0005	1.0006	1.0006	1.0006	1.0006
1.36	1.0031	1.0032	1.0032	1.0032	1.0032
1.90	1.0066	1.0065	1.0065	1.0064	1.0063
2.45	1.0119	1.0116	1.0114	1.0111	1.0111
2.99	1.0196	1.0188	1.0184	1.0183	1.0181
3.53	1.0320	1.0304	1.0296	1.0292	1.0292
3.80	1.0471	1.0444	1.0413	1.0350	1.0390
4.08	1.0673	1.0657	1.0629	1.0566	1.0516
4.21	1.1003	1.1014	1.0987	1.0878	1.0736

TABLE 2

RADIAL HEAT GENERATION IN THE OUTER MARK 15 SLUG

<u>Region</u>	<u>Normalized Value</u>
1	1.0033
2	1.0000
3	1.0116
4	1.0372
5	1.0807

TABLE 3

THERMAL CONDUCTIVITIES

<u>Material</u>	<u>Thermal Conductivity</u> <u>pcu/hr-ft-°C</u>
Aluminum	120
Aluminum Oxide ⁵	1.1
Uranium	17
Uranium oxide ⁶ at 300°C	3.15
Air	0.0303
Nickel oxide	0.3*

*Estimated by taking the thermal conductivity for pure nickel at 538°C and dividing by 100. The 100 factor is the ratio of aluminum and aluminum oxide thermal conductivity values.

TABLE 4

CONVECTION BOUNDARY CONDITIONS

<u>Assembly Power</u>	Coolant Temperature, °C		Convection Coefficient, pcu/hr-ft ² -°C	
	<u>Inner</u>	<u>Outer</u>	<u>Inner</u>	<u>Outer</u>
6.12	89	84	7132	6062
7.82	95	88	7650	6428

FIGURE 1

SCHEMATIC OF OUTER MARK 15 SLUG

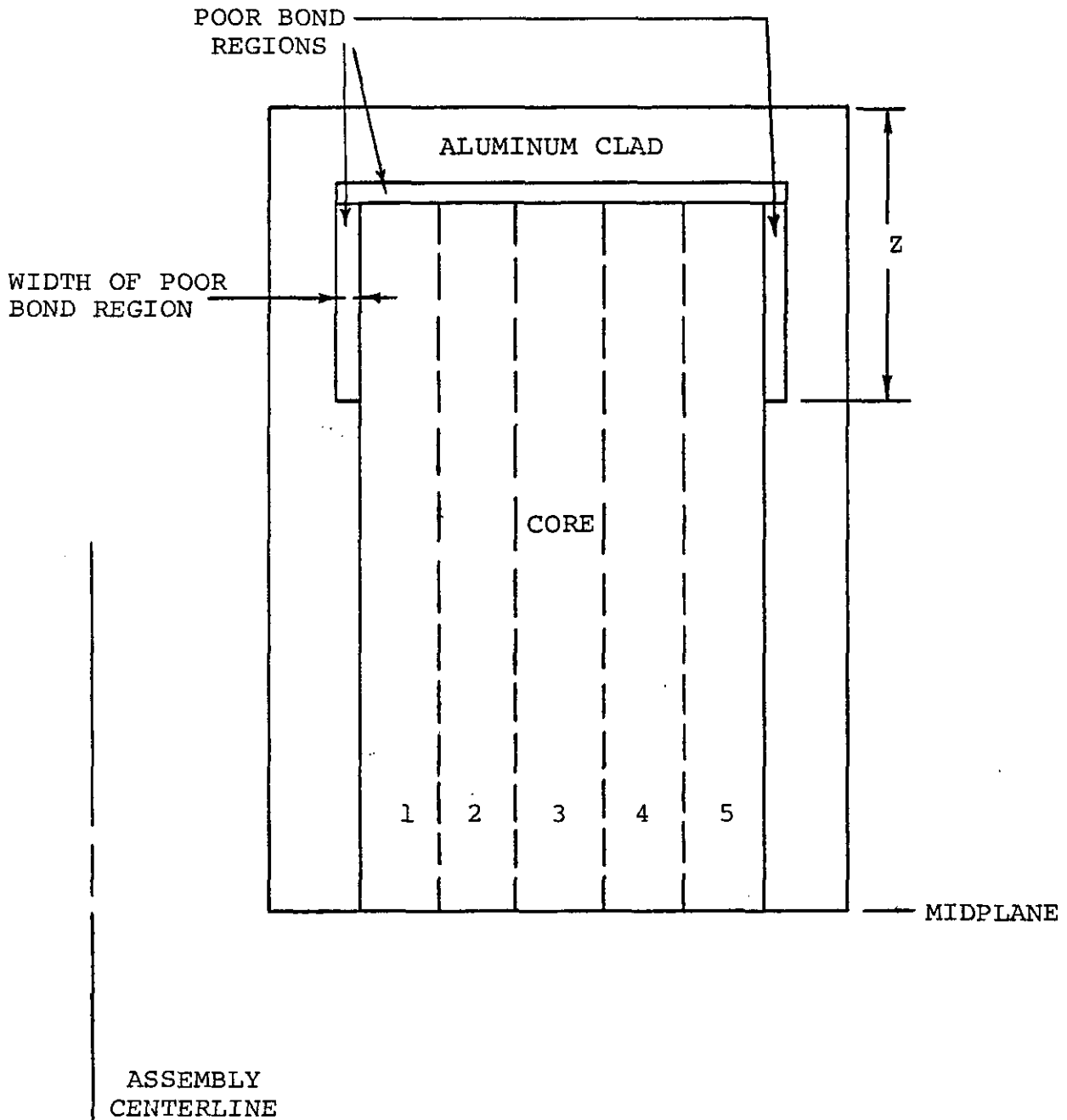


FIGURE 2

HEAT TRANSMISSION PATHS FOR A GOOD AND POOR BOND

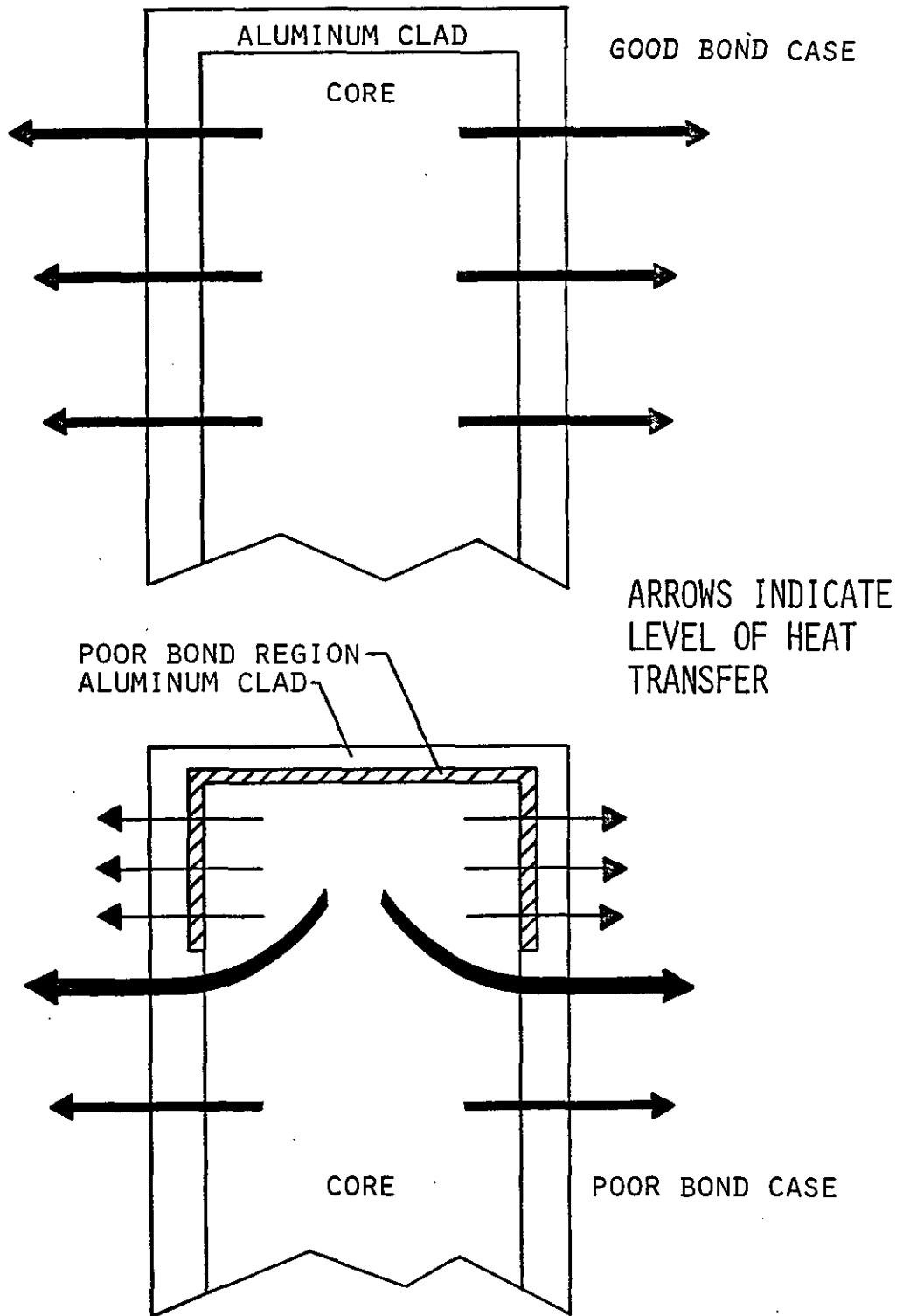


FIGURE 3

TEMPERATURE MAP FOR A NORMAL SLUG

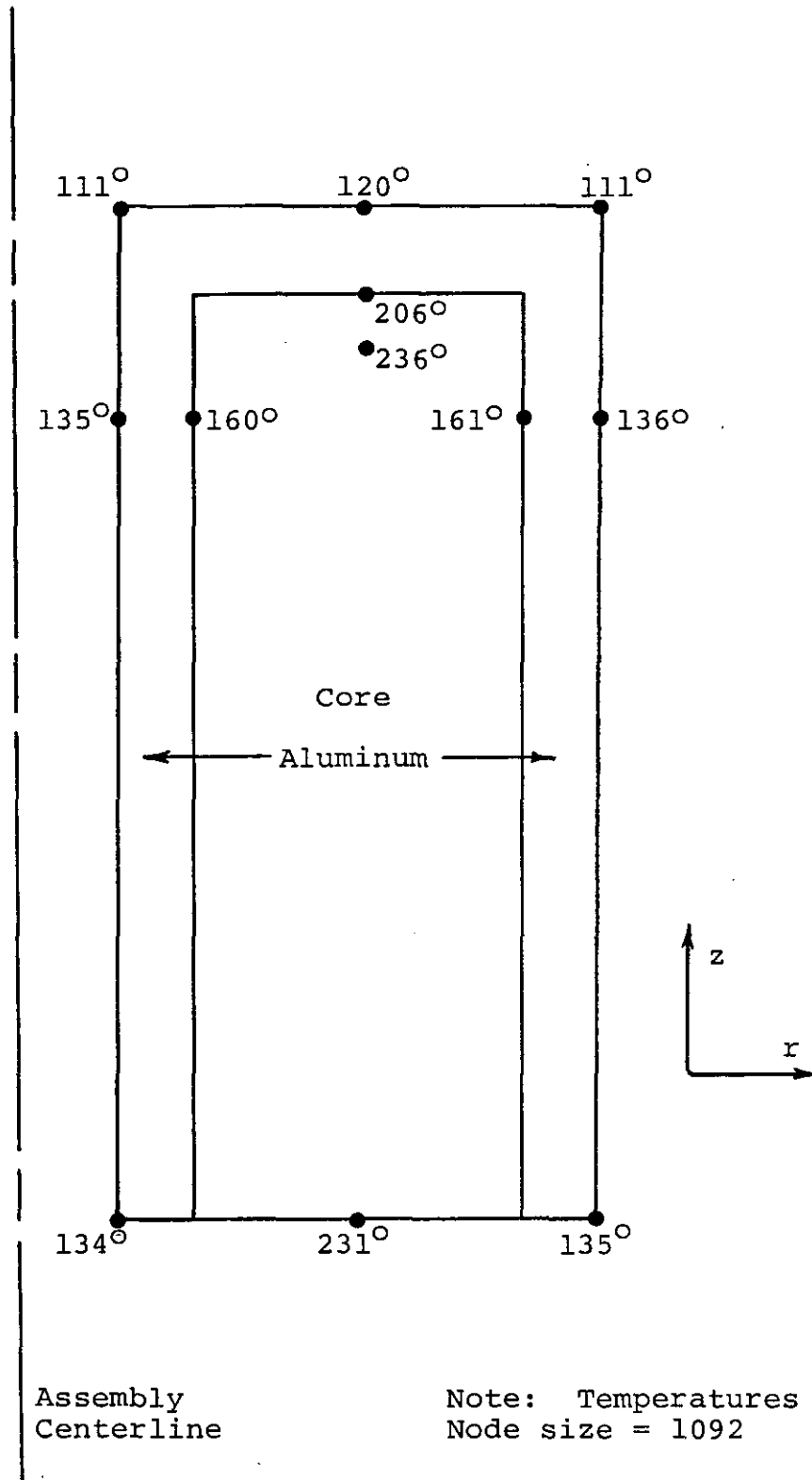


FIGURE 4

TEMPERATURE DISTRIBUTION ON INNER SURFACE FOR
A UNIFORM 0.5 MIL AIR GAP

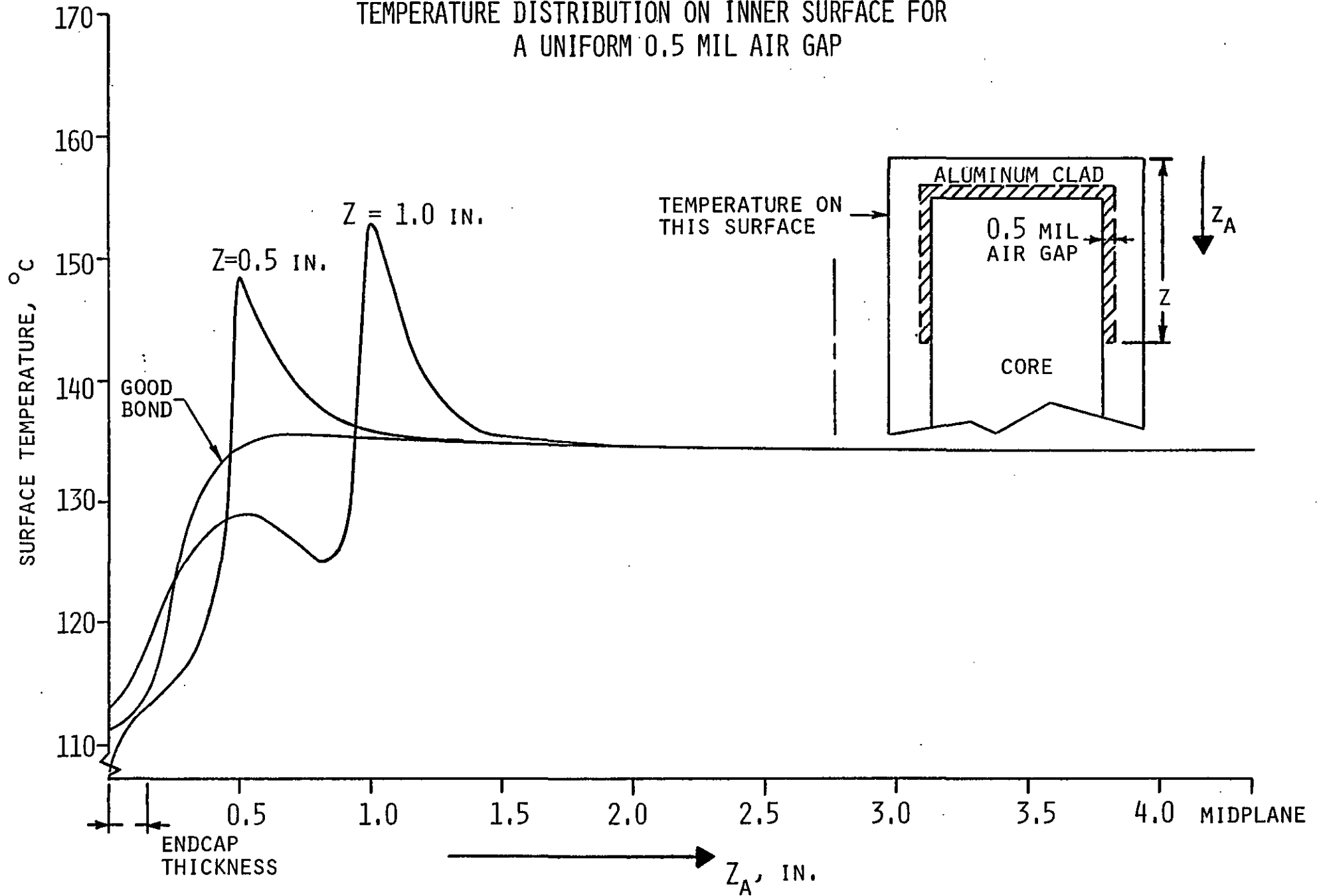


FIGURE 5
TEMPERATURE DISTRIBUTION ON
INNER SURFACE

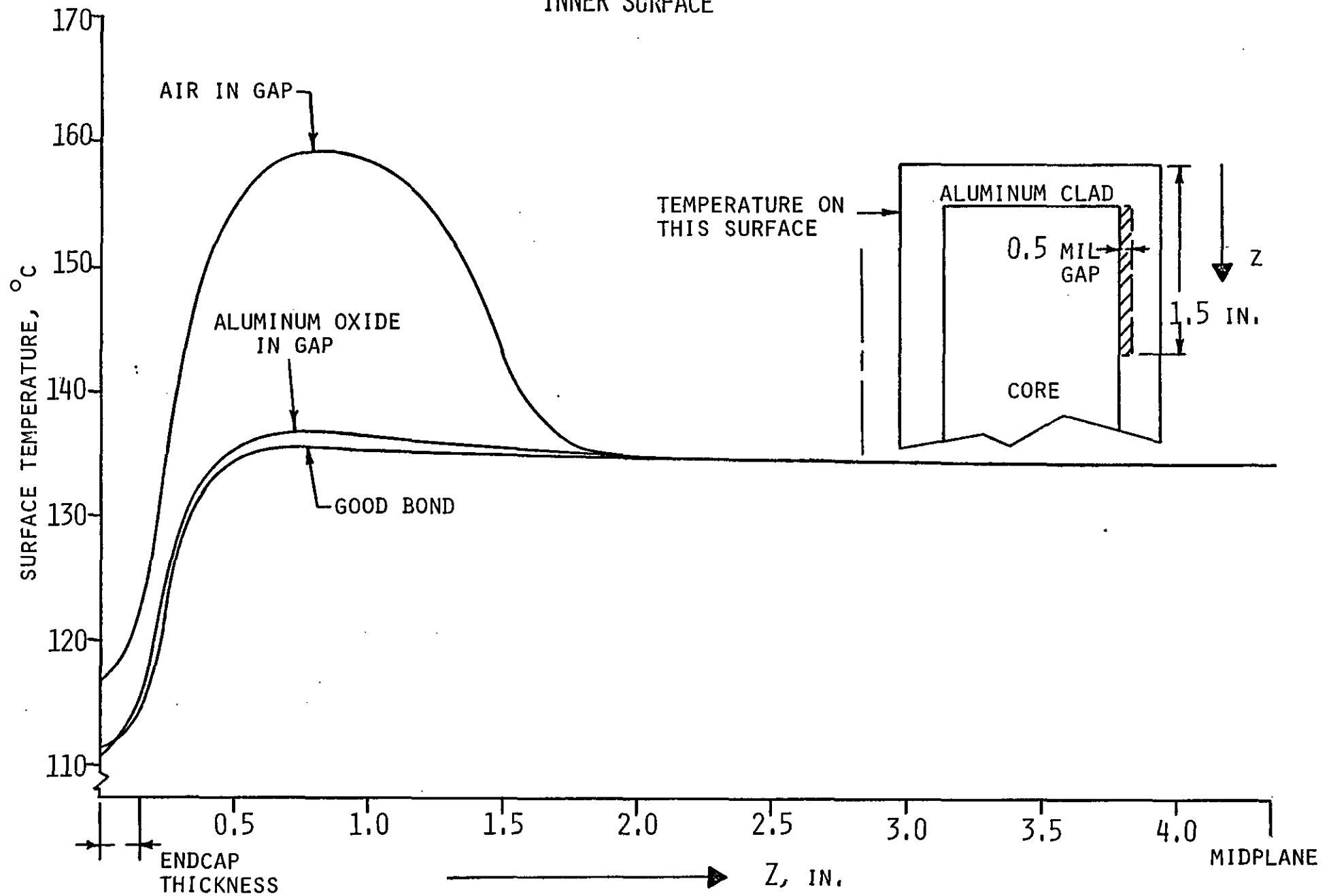
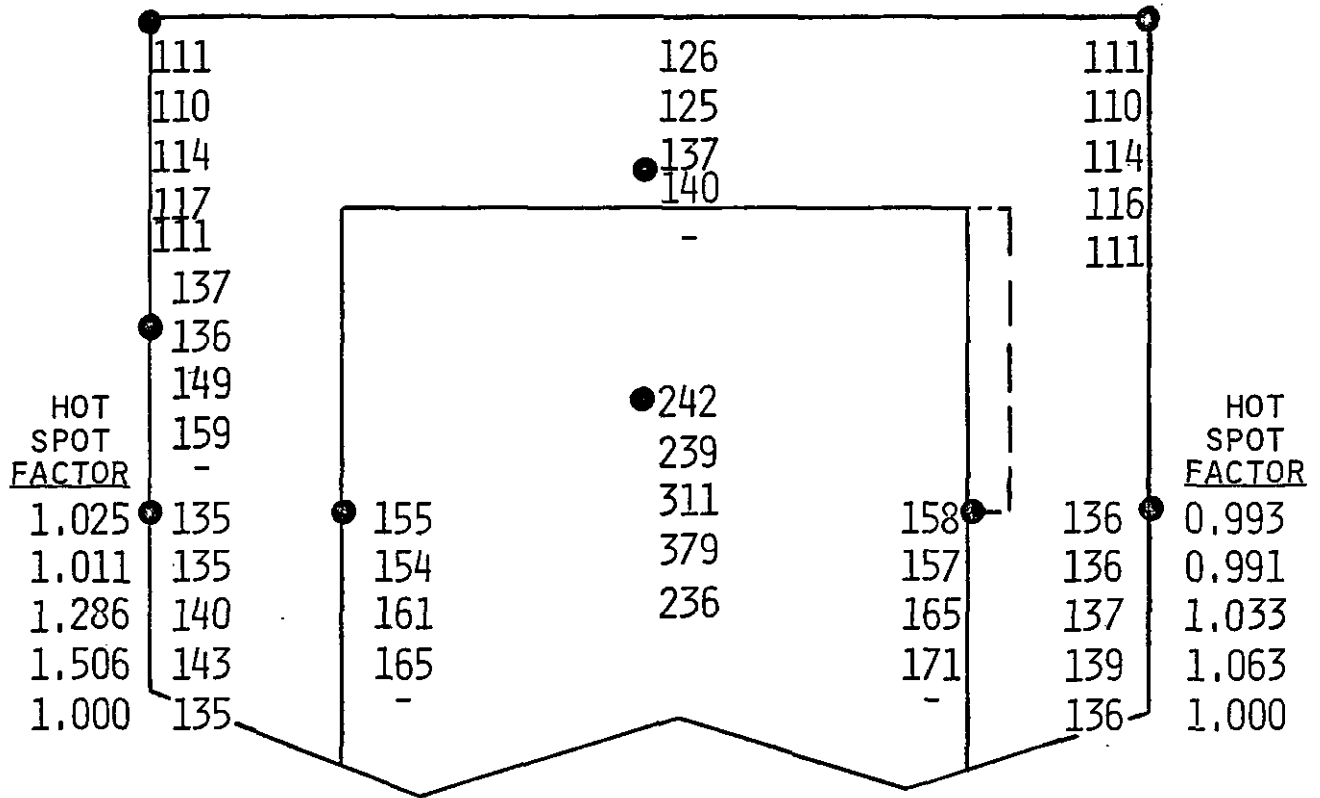


FIGURE 6
TEMPERATURE MAP FOR 6.12 MW POWER WITH ONE
POOR BOND REGION



POOR BOND PARAMETERS

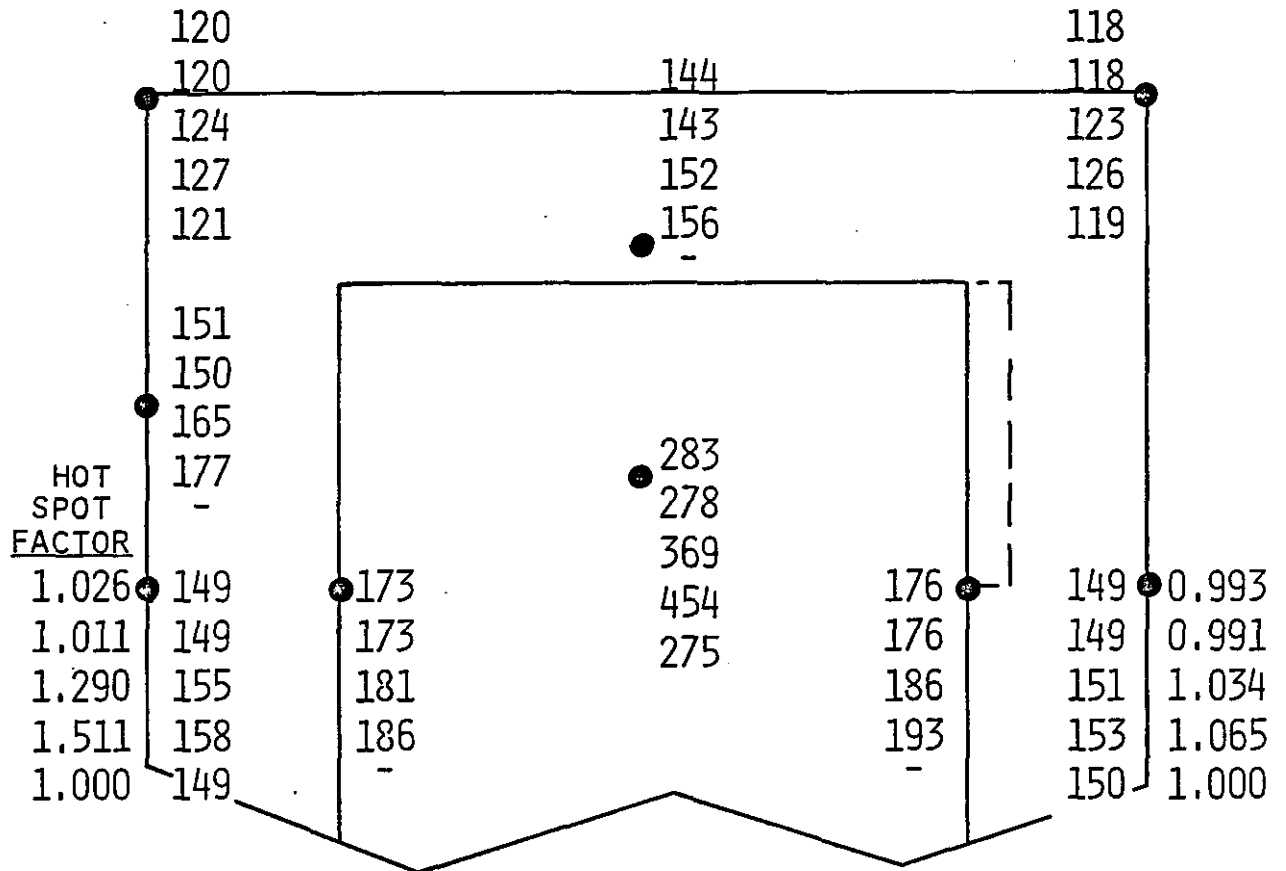
NUMBER OF NODES	Z (IN.)	GAP (MILS)	GAP MATERIAL	MATERIAL CONDUCTIVITY
2652	1.5	0.5	AL ₂ O ₃	1.1
2652	1.5	0.25	AL ₂ O ₃	1.1
2652	1.5	0.25	AIR	0.03
2652	1.5	0.5	AIR	0.03
1092			GOOD BOND	

ASSEMBLY CENTERLINE

POWER = 6.12 MW

ALL TEMPERATURES ARE IN DEGREES C.

FIGURE 7
 TEMPERATURE MAP FOR 7.82 MW POWER WITH ONE
 POOR BOND REGION



POOR BOND PARAMETERS

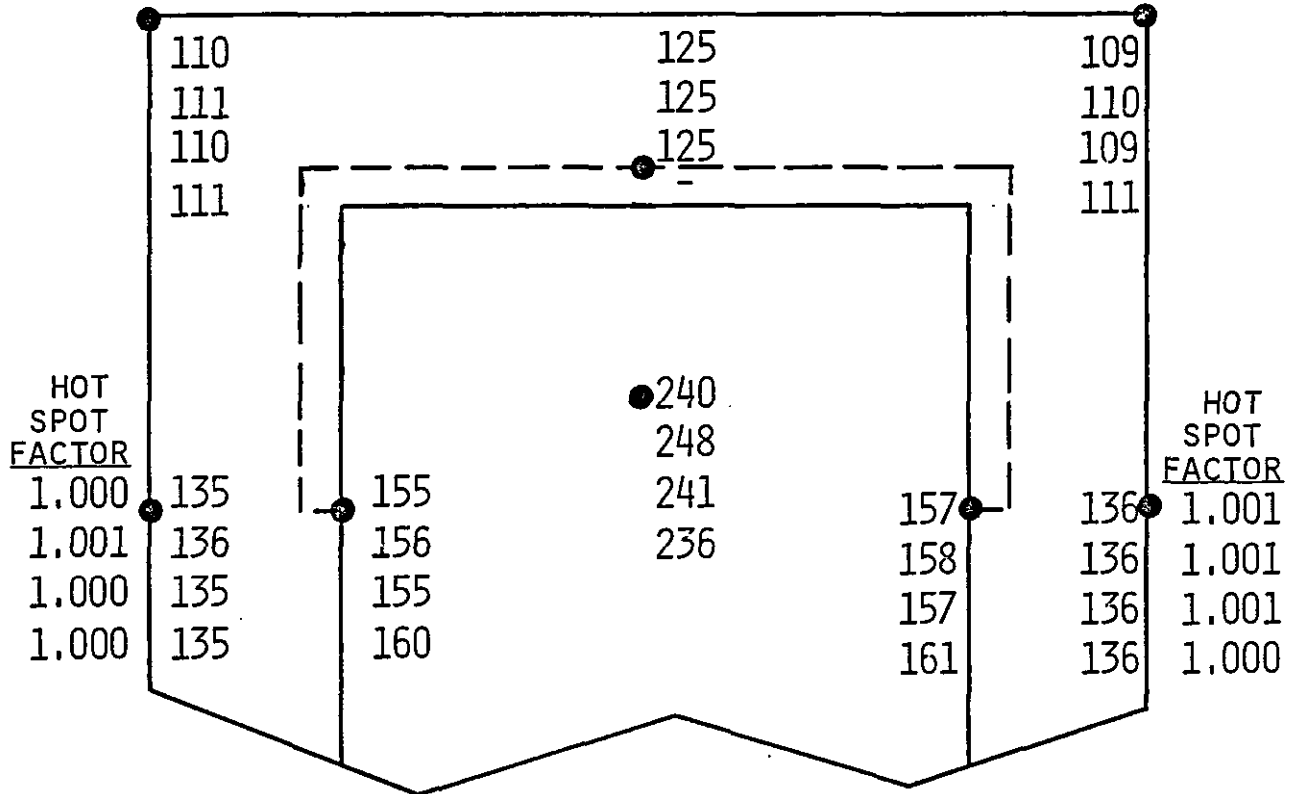
NUMBER OF NODES	Z (IN.)	GAP (MILS)	GAP MATERIAL	MATERIAL CONDUCTIVITY
2652	1.5	0.5	AL ₂ O ₃	1.1
2652	1.5	0.25	AL ₂ O ₃	1.1
2652	1.5	0.25	AIR	0.03
2652	1.5	0.5	AIR	0.03
1092			GOOD BOND	

POWER = 7.82 MW

ALL TEMPERATURES ARE IN DEGREES C.

ASSEMBLY CENTERLINE

FIGURE 8
TEMPERATURE MAP FOR OXIDES WITH THREE
POOR BOND REGIONS



POOR BOND PARAMETERS

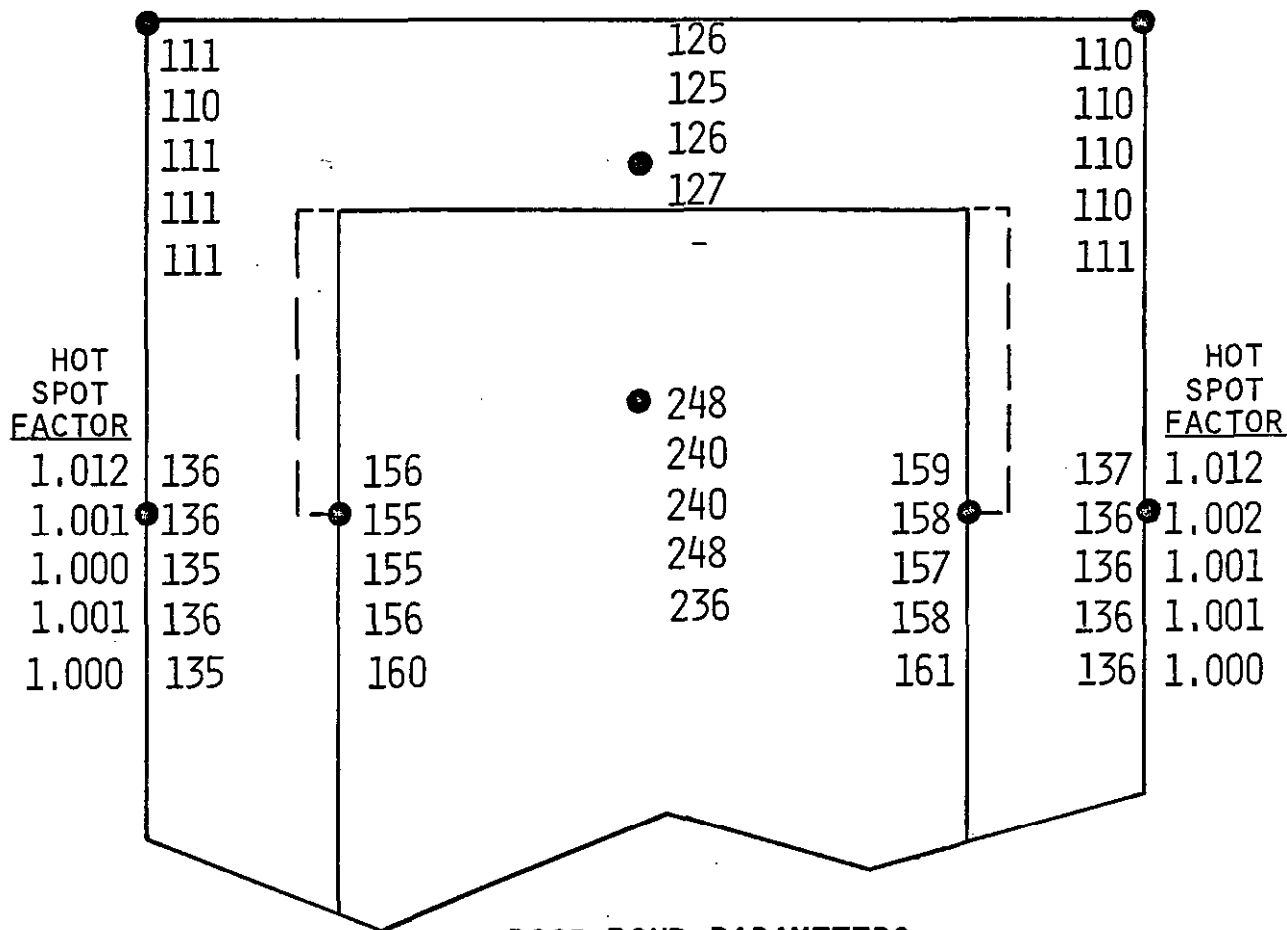
<u>NUMBER OF NODES</u>	<u>Z (IN.)</u>	<u>GAP (MILS)</u>	<u>GAP MATERIAL</u>	<u>MATERIAL CONDUCTIVITY</u>
2652	1.5	0.5	UO ₂	3.15
2652	1.5	0.5	AL ₂ O ₃	1.1
2652	1.5	0.25	AL ₂ O ₃	1.1
1092			GOOD BOND	

POWER = 6.12 MW

ALL TEMPERATURES ARE IN DEGREES C.

ASSEMBLY
CENTERLINE

FIGURE 9
TEMPERATURE MAP FOR OXIDES WITH TWO
POOR BOND REGIONS



POOR BOND PARAMETERS

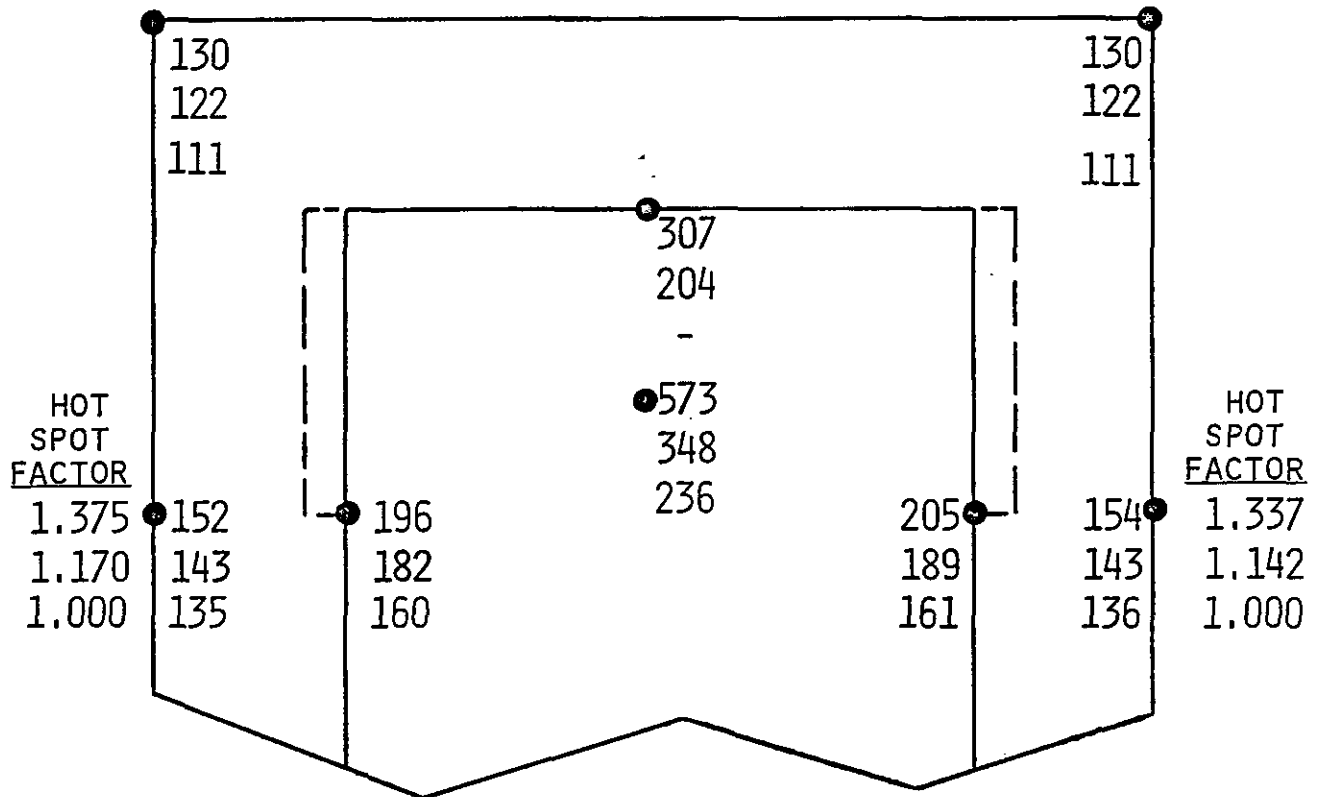
NUMBER OF NODES	Z (IN.)	GAP (MILS)	GAP MATERIAL	MATERIAL CONDUCTIVITY
2652	1.0	0.5	Al ₂ O ₃	1.1
2652	1.0	0.5	UO ₂	3.15
2652	1.5	0.5	UO ₂	3.15
2652	1.5	0.5	Al ₂ O ₃	1.1
1092			GOOD BOND	

POWER = 6.12 MW

ALL TEMPERATURES ARE IN DEGREES C.

ASSEMBLY
CENTERLINE

FIGURE 10
 TEMPERATURE MAP FOR AIR WITH TWO
 POOR BOND REGIONS



POOR BOND PARAMETERS

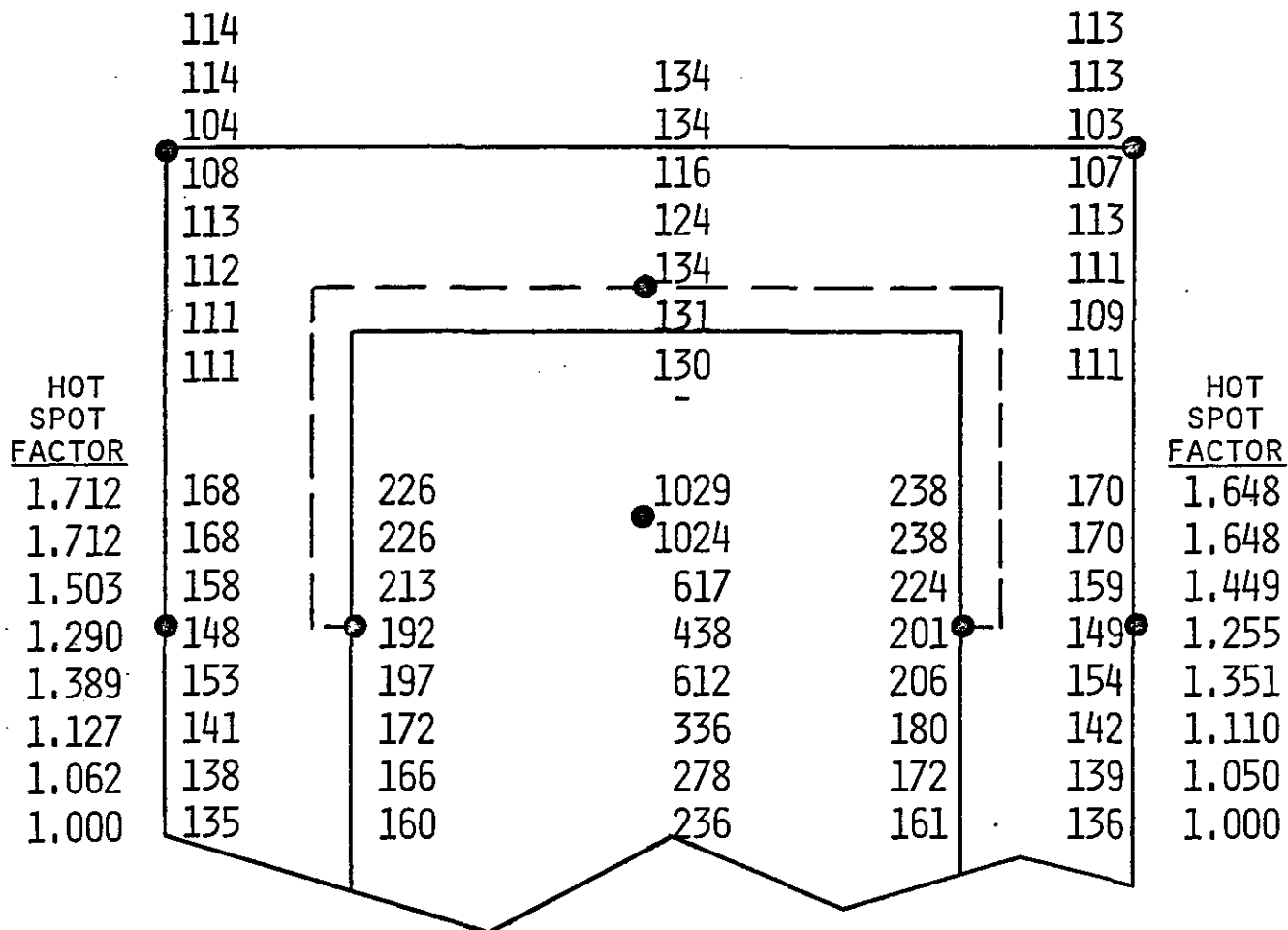
NUMBER OF NODES	Z (IN.)	GAP (MILS)	GAP MATERIAL
1242	1.0	0.5	AIR
1242	0.5	0.5	AIR
1092	GOOD BOND		

POWER = 6.12 MW

ALL TEMPERATURES ARE IN DEGREES C.

ASSEMBLY
 CENTERLINE

FIGURE 11
TEMPERATURE MAP FOR AIR WITH THREE POOR
BOND REGIONS



POOR BOND PARAMETERS

NUMBER OF NODES	Z (IN.)	GAP (MILS)	GAP MATERIAL
1053	1.0	1.2	AIR (NO RADIATIVE HEAT TRANSFER)
1053	1.0	1.2	AIR
1053	0.5	1.2	AIR
1053	0.5	0.5	AIR
1242	1.0	0.5	AIR
1053	1.0	1.2	NiO
1053	1.0	0.5	NiO
1092			GOOD BOND

ASSEMBLY CENTERLINE

POWER = 6.12 MW

ALL TEMPERATURES ARE IN DEGREES C.

FIGURE 12

BURNOUT RISK CURVES

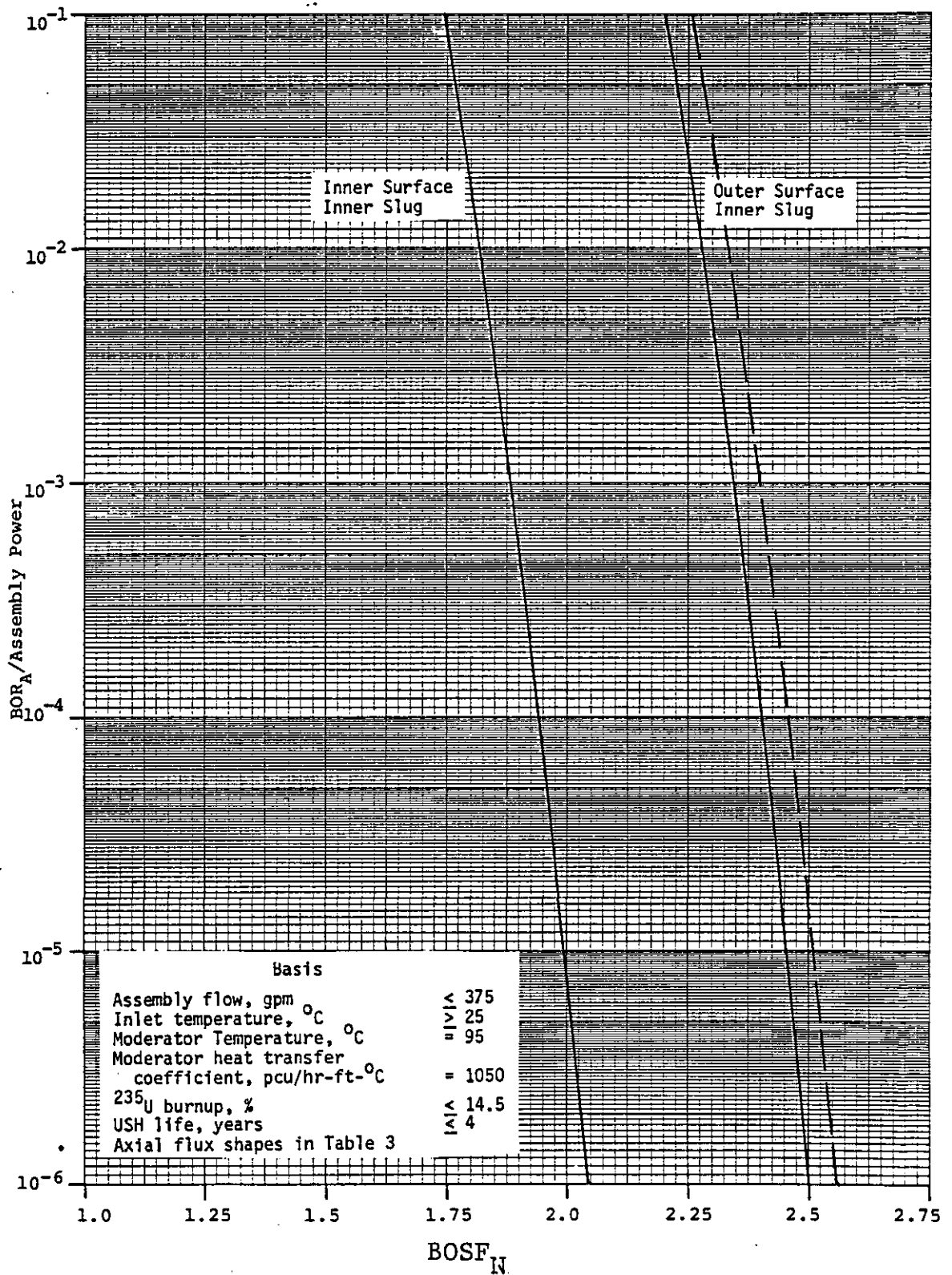
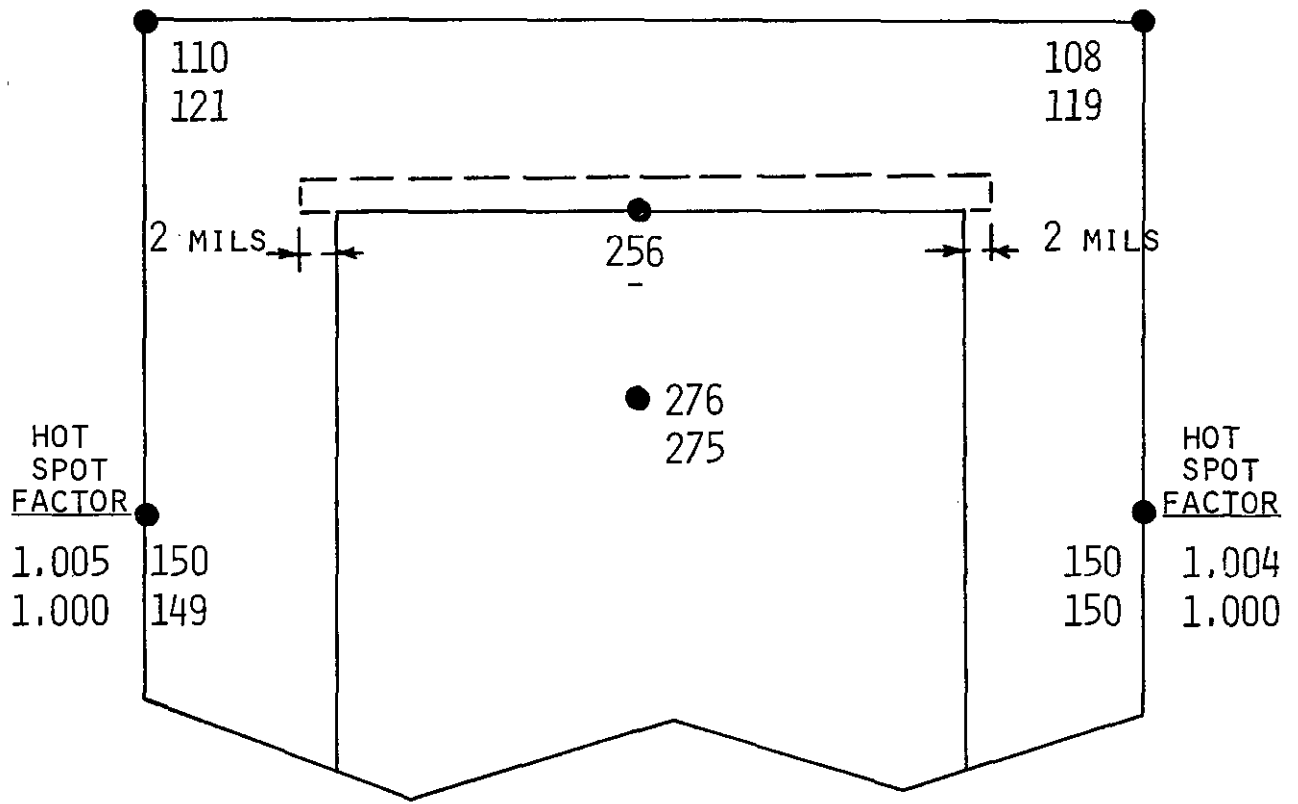


FIGURE 13
 TEMPERATURE MAP FOR 7.82 MW POWER
 WITH AIR GAP AT END OF CORE



POOR BOND PARAMETERS

<u>NUMBER OF NODES</u>	<u>Z (IN.)</u>	<u>GAP (MILS)</u>	<u>GAP MATERIAL</u>	<u>MATERIAL CONDUCTIVITY</u>
2652	-	2.0	AIR	0.03

GOOD BOND

ASSEMBLY
 CENTERLINE

POWER = 7.82 MW

ALL TEMPERATURES ARE IN DEGREES C.